The deletion of the protein phosphatase 1 regulator NIPP1 in testis causes hyperphosphorylation and degradation of the histone methyltransferase EZH2

Received for publication, August 30, 2018, and in revised form, September 25, 2018 Published, Papers in Press, October 10, 2018, DOI 10.1074/jbc.AC118.005577

Mónica Ferreira[‡§], **Iris Verbinnen**[‡], **Margarida Fardilha**[§], **Aleyde Van Eynde**[‡1], **and Mathieu Bollen**[‡2]

From the [‡]*Laboratory of Biosignaling & Therapeutics, KU Leuven Department of Cellular and Molecular Medicine, University of Leuven, B-3000 Leuven, Belgium and* [§]*Institute for Research in Biomedicine (iBiMED), Health Sciences Department, University of Aveiro, 3810 Aveiro, Portugal*

Edited by John M. Denu

Germ cell proliferation is epigenetically controlled, mainly through DNA methylation and histone modifications. However, the pivotal epigenetic regulators of germ cell self-renewal and differentiation in postnatal testis are still poorly defined. The histone methyltransferase enhancer of zeste homolog 2 (EZH2) is the catalytic subunit of Polycomb repressive complex 2, represses target genes through trimethylation of histone H3 at Lys-27 (H3K27me3), and interacts (in)directly with both protein phosphatase 1 (PP1) and nuclear inhibitor of PP1 (NIPP1). Here, we report that postnatal, testis-specific ablation of NIPP1 in mice results in loss of EZH2 and reduces H3K27me3 levels. Mechanistically, the NIPP1 deletion abrogated PP1-mediated EZH2 dephosphorylation at two cyclin-dependent kinase sites (Thr-345/487), thereby generating hyperphosphorylated EZH2, which is a substrate for proteolytic degradation. Accordingly, alanine mutation of these residues prolonged the half-life of EZH2 in male germ cells. Our study discloses a key role for the PP1:NIPP1 holoenzyme in stabilizing EZH2 and maintaining the H3K27me3 mark on genes that are important for germ cell development and spermatogenesis.

The postnatal proliferation and differentiation of germ cells is epigenetically controlled, mainly through DNA methylation and covalent histone modifications (1–3). This implies a tight regulation of the concentration, chromatin targeting, and catalytic activity of DNA- and histone-modifying enzymes. The key epigenetic regulators of self-renewal and differentiation in germ cells of postnatal testis are still poorly defined (1–4). One notable exception is the Polycomb repressive complex 2 (PRC2), which is essential for the maintenance of male germ cells (5, 6). The PRC2 complex contributes to the transcriptional silencing of Polycomb group (PcG)[3] target genes, which control pluripotency, cell proliferation, and differentiation (7, 8). EZH2 (enhancer of zeste homolog 2) is the catalytic subunit of the PRC2 complex and di/trimethylates histone H3 at Lys-27 (H3K27me2/3). The noncatalytic PRC2 core components comprise SUZ12 (suppressor of zeste homolog 12), EED (embryonic ectoderm development), and RBAP48 (retinoblastoma-associated protein of 48 kDa), which all promote methylation by EZH2. PRC2 represses the transcription of PcG targets mainly because the deposited H3K27me3 hampers the recruitment of ATP-dependent chromatin-remodeling complexes and RNA polymerase II (7–9).

PRC2-mediated gene silencing is antagonistically regulated by cyclin-dependent kinases 1/2 (CDK1/2) and protein phosphatase 1 (PP1), which (de)phosphorylate EZH2 at Thr-345, Thr-416, and Thr-487 (mouse residues used throughout this manuscript) (10–13). Phosphorylation at Thr-345 increases the targeting of EZH2 to chromatin, resulting in enhanced H3K27 di/trimethylation at target loci (10, 11). EZH2 phosphorylation at Thr-487 and prolonged phosphorylation at Thr-345 was linked to its proteasomal degradation in late mitosis (14). Thr-487 phosphorylation has been reported to disrupt the interaction of EZH2 with other PRC2 components (15), but this is not a general finding (11). Anyhow, free EZH2 is ubiquitinated by the SCF-type E3-ubiquitin ligase β-TrCP (FBXW1), in particular when it is also phosphorylated by Jak2 at Tyr-641, leading to its proteasomal degradation (16). Finally, the CDK-mediated phosphorylation of EZH2 at Thr-416 creates a docking site for NIPP1 (nuclear inhibitor of PP1), which regulates the dephosphorylation of CDK sites by PRC2-associated PP1 (12). The essential role of NIPP1 in PRC2 signaling is also underscored by other studies. Thus, NIPP1 has direct interaction sites for both EZH2 and EED (12, 17) and acts as a transcriptional repressor in a PRC2-dependent manner (17, 18). In addition, NIPP1 binds to a subset of PcG target genes and promotes the association of EZH2 with proliferation-related target genes (12, 19, 20). Finally, the importance of NIPP1 in PcG signaling was recently substantiated by its identification in an unbiased shRNA screen for modifiers of Polycomb silencing (21) as well as by enhanced levels

This work was supported by the Fonds Wetenschappelijk Onderzoek G078717N and by the Bijzonder Onderzoeksfonds (BOF-GOA 10/18). This work was also supported by a doctoral fellowship from FCT/Portuguese Ministry of Science and Technology (MEC Fundação para a Ciência e a Tecnologia (FCT)) (to M. F.). The authors declare that they have no conflicts of interest with the contents of this article.

This article contains Figs. S1 and S2.

Gene expression data are available at GEO under the accession number GSE83145.

[1] To whom correspondence may be addressed: Campus Gasthuisberg, Herestraat 49, O&N1, PB901, B-3000 Leuven, Belgium. Tel.: 32-16-33-02-90; E-mail: Aleyde.VanEynde@kuleuven.be.

[2] To whom correspondence may be addressed: Campus Gasthuisberg, Herestraat 49, O&N1, PB901, B-3000 Leuven, Belgium. Tel.: 32-16-33 06 44; E-mail: Mathieu.Bollen@kuleuven.be.

[3] The abbreviations used are: PcG, Polycomb group; FHA, forkhead-associated (domain); iKO, induced knockout; CTR, control; FPKM, fragments per kilobase of exon per million fragments mapped.

of H3K27me3 upon the expression of a functionally validated PP1-NIPP1 fusion in HeLa cells (22).

NIPP1, encoded by *Ppp1r8*, is one of nearly 200 known regulatory interactors of PP1 (RIPPOs) in vertebrates (23). It is a nuclear protein of 38 kDa comprising an N-terminal forkhead-associated (FHA) domain, a central PP1-anchoring domain, and a C-terminal PP1-inhibitory domain. The FHA domain has a phosphate-binding loop that binds proteins, including EZH2, that are phosphorylated on specific phospho-Thr-Pro (pTP) dipeptide motifs by CDKs (12). Full-length NIPP1 is a potent inhibitor of PP1 toward all tested substrates, but allows the controlled dephosphorylation of phosphoproteins that are recruited via the FHA domain (24–26). Efficient dephosphorylation of FHA ligands by NIPP1-associated PP1 requires the allosteric removal of the C-terminal PP1-inhibitory domain of NIPP1 but the underlying mechanism is poorly understood (24).

Using an inducible NIPP1 knockout (iKO) model, we have demonstrated that NIPP1 is essential for mammalian spermatogenesis and, more specifically, is required for the transcriptional regulation of genes implicated in germ cell proliferation and survival (27). In this study, we used this iKO model to show that the deletion of NIPP1 in testis is associated with the loss of EZH2 and a reduced histone H3K27 trimethylation at target genes. The deficiency of EZH2 is explained by its enhanced phosphorylation at CDK sites, because of a loss of functional PP1:NIPP1, which promotes its proteolytic degradation. Our findings indicate that NIPP1 is not only an inhibitor of PP1 but also allows the timely dephosphorylation of EZH2 by associated PP1. We also discuss to which extent the loss of EZH2 may contribute to the observed testis phenotype of the NIPP1 iKOs.

Results

The ablation of NIPP1 in testis results in a loss of PRC2 core components

At the age of 4 weeks mice harboring the *Ubc-Cre-ERT2* transgene, one floxed *Pppr8* allele, and either a WT (CTR) or knockout (iKO) *Ppp1r8* allele were injected with tamoxifen at days 1, 3, 5, and 7 to excise the floxed *Ppp1r8* region. The animals were sacrificed 2 weeks from the beginning of this treatment, when they reached the age of 6 weeks. At this stage, a histological phenotype cannot yet be discerned in the iKOs (27). However, the NIPP1 protein level in their testis was already reduced by about 70%, as compared with its level in CTR mice (Fig. 1, *A* and *B*). Intriguingly, although the deletion of NIPP1 was not associated with an altered level of the FHA ligands CDC5L and SAP155 (Fig. S5 in Ref. 27), it did result in the down-regulation of the FHA ligand EZH2 by some 40%, as determined by both immunoblotting (Fig. 1, *A* and *C*) and immunostaining (Fig. 1*H*). Consistent with multiple reports showing that the loss of one PRC2 core component also destabilizes other PRC2 subunits (28–31), the levels of the PRC2 subunits RBAP48 and SUZ12 were also reduced by 30–40% in the NIPP1 iKOs (Fig. 1, *A*, *D*, *E*, and *H*). RNA-Seq did not disclose altered transcript levels of the examined PRC2 core components in the iKOs (Fig. 1*F*), suggesting that their decreased level involves a (post) transcriptional process. We confirmed by co-immunoprecipitation analysis that NIPP1 and EZH2 are part of the same macromolecular complex in nuclear extracts of testis (Fig. 1*G*), as already demonstrated previously for HeLa cells (12). Collectively, these data suggested that the depletion of NIPP1 in testis results in the loss of EZH2 and the associated destabilization of its regulatory subunits.

Deficient PRC2 levels correlate with the deregulation of target genes

We proceeded to explore the consequences of the loss of PRC2 core components in the testis of NIPP1 iKOs. As expected, the testicular level of H3K27me3 in these mice was significantly reduced, as shown by both immunostaining (Fig. 2*A*) and immunoblotting (Fig. 2, *B* and *C*). Close inspection of the immunostainings revealed that the loss of H3K27me3 in the iKOs was stage-dependent and most prominent at the early and middle stages of the spermatogenic cycle (Fig. 2*A*). We have verified that the proportion of tubes at different stages of development is not altered between iKOs and CTRs (27). Based upon lists of previously identified PcG target genes (5, 32–34), 12% of the 17,344 mouse genes mapped by comparative RNA-Seq profiling (27) were identified as likely PcG targets (Fig. 2*D*). Using the same criteria, 26% of the 274 genes that were down- or up-regulated in the NIPP1 iKOs were classified as likely PcG targets, reflecting a more than 2-fold enrichment over their genome-wide occurrence. The up-regulated PcG genes included the pro-apoptotic gene *Bbc3* as well as genes that are involved in cell-cycle progression (*Tnk1, Dtx3l*, and *Kif2b*) and gonadal development (*Lhx9*) (Fig. 2*E*). Among the down-regulated PcG targets were genes associated with cell-cycle progression (*Cdkn2a*, *Kntc1*) and the POU transcription factor *Pou3f3*, which is involved in the development of several tissues. In general, these altered expression profiles were consistent with the observed decreased proliferation and survival potential of testicular iKO germ cells (Fig. 6, *e* and *f* in Ref. 27). We verified by ChIP analysis that H3K27me3 was enriched at or around the promoter region of key PRC2 target genes in testis (Fig. 2*F*) and that the deletion of NIPP1 was associated with decreased H3K27 trimethylation at these loci, except for *Cdkn2a* (Fig. 2*G*). Paradoxically, the decreased H3K27me3 level of *Pou3f3* correlated with a decreased transcript level, indicating that *Pou3f3* expression is also regulated by non–PcG-related mechanisms or belongs to the subgroup of PcG targets that are activated (19, 35) by distinct mechanisms, including EZH2-dependent methylation of transcription factors or transcription elongating factors (36, 37). Together, these data functionally validated the loss of PRC2 components in the NIPP1 iKOs.

Hyperphosphorylation and enhanced degradation of EZH2 in the NIPP1 iKOs

In HeLa cells EZH2 is targeted for proteasomal degradation following its CDK1/2-mediated phosphorylation at Thr-345 and Thr-478 (14, 15). This led us to hypothesize that the deletion of NIPP1 results in a deficient targeting of PP1 to EZH2, resulting in the hyperphosphorylation and destabilization of EZH2. To explore this hypothesis, we first compared the half-lives of EGFP-tagged EZH2-WT, EZH2-T345A, and EZH2-T487A that were transiently expressed in a spermatogonial cell line (C18-4), after the addition of the protein synthesis inhibitor

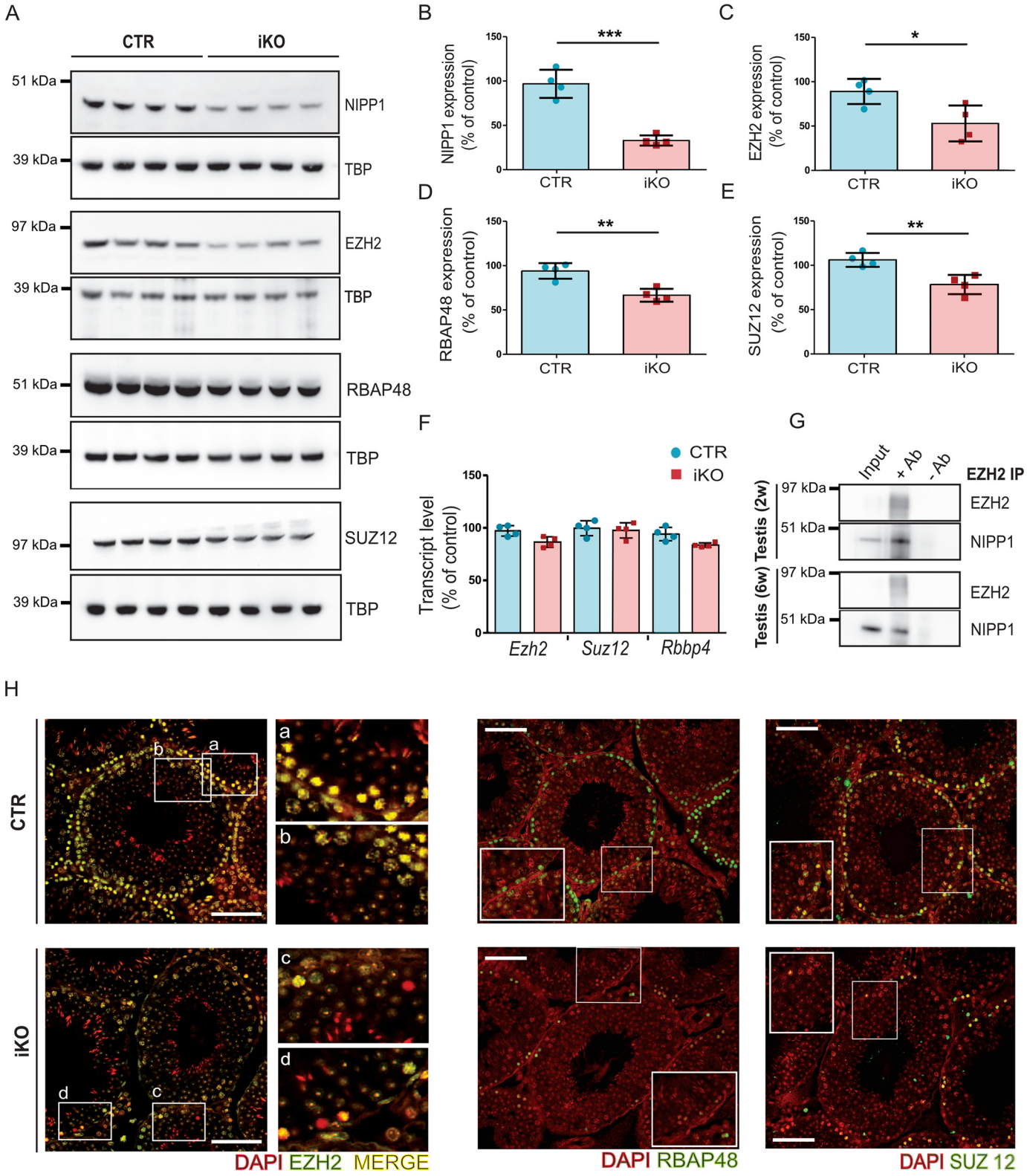

Figure 1. The deletion of NIPP1 results in the destabilization of PRC2 core components. *A*, NIPP1, EZH2, RBAP48, and SUZ12 levels were detected by immunoblotting. TBP was used as a loading control. *B–E*, quantification of the NIPP1, EZH2, RBAP48, and SUZ12 protein levels as shown in *panel A*. *F*, expression of the indicated genes in tamoxifen-treated CTR and iKO mice of 6 weeks, as derived from RNA-Seq data. All bar data are mean ± S.D. ($n = 4$ animals per experimental group). *, $p < 0.05$; **, $p < 0.01$, ***, $p < 0.001$. *G*, Immunoprecipitates (*IP*) of endogenous EZH2 from testis homogenates of 2- and 6-week-old CTR mice were immunoblotted for co-immunoprecipitated NIPP1. *W*, weeks; + *Ab*, EZH2 antibody added; − *Ab*, no antibody added. *H*, testis sections of tamoxifen-injected mice of 6 weeks were immunostained for EZH2, RBAP48, and SUZ12. *Scale bar*, 50 μm.

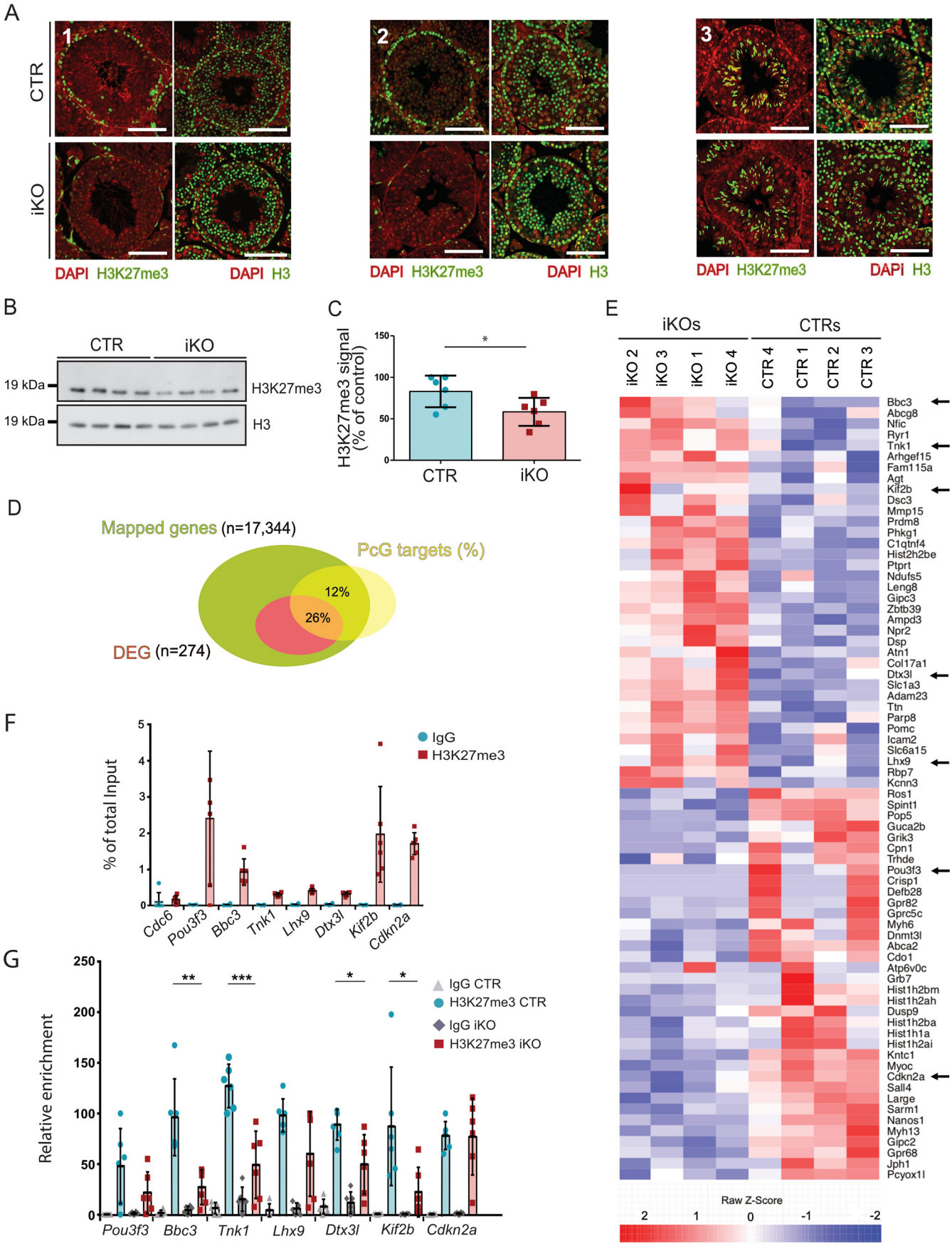
A
CTR
iKO
1
2
3
DAPI H3K27me3
DAPI H3
B
CTR
iKO
19 kDa
H3K27me3
H3
C
H3K27me3 signal (% of control)
CTR
iKO
D
Mapped genes (n=17,344)
PcG targets (%)
12%
26%
DEG (n=274)
E
iKOs
CTRs
iKO 2
iKO 3
iKO 1
iKO 4
CTR 4
CTR 1
CTR 2
CTR 3
Raw Z-Score
F
% of total Input
IgG
H3K27me3
Cdc6
Pou3f3
Bbc3
Tnk1
Lhx9
Dtx3l
Kif2b
Cdkn2a
G
Relative enrichment
IgG CTR
H3K27me3 CTR
IgG iKO
H3K27me3 iKO
Pou3f3
Bbc3
Tnk1
Lhx9
Dtx3l
Kif2b
Cdkn2a

cycloheximide (Fig. 3, *A–C*). EZH2-WT had a half-life of ~2 h, but this increased to about 6 h for the nonphosphorylatable alanine mutants, similar to the half-life of EGFP. Thus, EZH2 in C18-4 cells is stabilized by preventing phosphorylation at Thr-345 or Thr-487. Next, we examined whether these sites are hyperphosphorylated in testis of the NIPP1 iKOs. Because Thr-345 and Thr-487 are followed by a proline, their phosphorylation status can be derived from immunoblotting with a pan pTP antibody, in particular because these residues represent the major TP-phosphorylation sites of EZH2 (10–13). EZH2 that was immunoprecipitated from testis lysates was hyperphosphorylated at TP-dipeptide motifs in the iKOs (Fig. 3, *D* and *E*). Moreover, EGFP-EZH2 that was ectopically expressed in C18-4 cells showed a significantly reduced phosphorylation at TP-dipeptide motifs (~70%) after the co-expression of a FLAG-tagged PP1-NIPP1 fusion. We have previously demonstrated that a PP1-NIPP1 fusion behaves as the native PP1:NIPP1 holoenzyme with respect to subcellular localization and enzymic properties (22, 38) and, unlike ectopically expressed NIPP1, does not competitively disrupt other PP1 holoenzymes (22, 39). The co-expression of a hypoactive fusion (PP1m-NIPP1), with a mutated metal-coordinating residue (D64A) in the active site of the PP1γ moiety that reduces its catalytic activity by 80–90% (22, 38), only had a mild effect (~20% reduction) on TP-dipeptide phosphorylation of EZH2 (Fig. 3, *F–H*). These data provide good evidence that EZH2 is a substrate for regulated dephosphorylation by PP1:NIPP1, in accordance with previous *in vitro* data (12). Thus, the loss of EZH2 in the testis of NIPP1 iKOs can be explained by deficient PP1-mediated dephosphorylation of its CDK sites, resulting in its hyperphosphorylation and proteasomal degradation.

Discussion

RIPPOs spatiotemporally control PP1, mainly through (i) targeting of the phosphatase to a subcellular compartment that contains substrates, (ii) direct recruitment of a subset of PP1 substrates, and/or (iii) activity modulation of associated PP1 (40). Full-length recombinant NIPP1 inhibits PP1 toward all tested substrates (24). However, the heterodimeric PP1:NIPP1 holoenzyme can be "de-inhibited" to allow dephosphorylation of NIPP1-associated FHA ligands, including SAP155 (25, 38) and EZH2 (this work). *In vitro* studies suggested that this de-inhibition may involve the allosteric removal of the C-terminal tail of NIPP1 from the active site of PP1, as can be induced by tyrosine phosphorylation or RNA binding of the C terminus (24) (Fig. 4). Although the physiological trigger(s) and mechanistic details of this putative allosteric regulation of PP1:NIPP1 are still unknown, our present work demonstrates that the dephosphorylation of EZH2 requires both NIPP1 and PP1, as EZH2 becomes hyperphosphorylated in the absence of NIPP1. Our data therefore validate NIPP1 as a canonical regulator of PP1, in that it acts inhibitory or facilitatory for dephosphorylation of FHA ligands by associated PP1, depending on the status of hitherto unknown upstream NIPP1-directed signaling.

The functional consequence of PP1:NIPP1-mediated dephosphorylation is clearly substrate dependent. Dephosphorylation of SAP155 affects its function as a splicing factor (25), but does not change its cellular concentration (38). Here, we demonstrated that EZH2 is hyperphosphorylated and targeted for proteolytic degradation in the absence of NIPP1. However, the *in vivo* regulation of EZH2 by PP1:NIPP1 is likely to be more dynamic and dependent on the functional status (inhibitory or facilitatory) rather than the concentration of NIPP1. We envisage that CDK1/2 phosphorylate EZH2 at Thr-345 to target it to specific chromatin loci (Fig. 4). Immediate dephosphorylation of this site is prevented by the simultaneous phosphorylation of EZH2 by CDK1/2 at Thr-416 (12), resulting in the recruitment of NIPP1 and the inhibition of PRC2-associated PP1 (Fig. 4). Here, NIPP1 serves to prolong the association of EZH2 with a subset of target genes, thereby enhancing the deposition of H3K27me3 at these loci (12, 19, 20). Consistent with this notion, we recently demonstrated that the expression of a PP1-NIPP1 fusion in HeLa cells augmented H3K27me3 levels at chromatin (22), confirming that this phosphatase can function as a positive regulator of EZH2 signaling. Prolonged phosphorylation of EZH2 at Thr-345 and Thr-487, as may occur during mitosis (14) or after the deletion of NIPP1 (this work), targets the affected pool of EZH2 for proteolytic degradation. Taken together, our data suggest that NIPP1 spatiotemporally controls the phosphorylation status of EZH2, either by blocking or facilitating its dephosphorylation by associated PP1.

The deletion of NIPP1 in testis resulted in a reduced proliferation and survival capacity of cells of the spermatogenic lineage, culminating in the total loss of germ cells by the age of 12 weeks (27). However, the testicular ablation of EZH2 elicited a much milder phenotype (5), demonstrating that its loss in the NIPP1 iKOs cannot fully account for the much stronger phenotype in the iKOs. The loss of EZH2 in testis is largely compensated for by its homolog EZH1 (6). Also, the combined deletion of EZH1 and EZH2 (6), or the ablation of the PRC2 components SUZ12 or EED (5), elicited a much stronger phenotype than that associated with EZH2-depleted testis. Because the residue of EZH2 (Thr-416) that mediates targeting to NIPP1 is conserved in EZH1, it will be interesting to examine whether the deletion of NIPP1 also affects EZH1

Figure 2. The loss of PRC2 core components correlates with reduced H3K27me3 levels and deregulation of target genes. *A*, testis sections of tamoxifen-treated mice of 6 weeks were immunostained for H3K27me3. Shown are seminiferous tubules at (1) early, (2) mid, and (3) late stages of the spermatogenic cycle. *Scale bar*, 50 μm. *B*, total H3 and H3K27me3 in histone extracts of testis were visualized by immunoblotting. *C*, quantification of H3K27me3, as shown in *panel B*. The results represent mean ± S.D. ($n = 6$ animals per experimental group). *D*, schematic representation of PcG target gene abundance (%) in the mapped testis genome (17,344 genes analyzed) and in 274 differentially expressed genes (*DEG*) in the testis of NIPP1 iKO mice as compared with CTR mice. *E*, comparative RNA-Seq profiling in testis of tamoxifen-treated mice of 6 weeks. The heat map shows significantly up- and down-regulated PcG target genes. *Arrows* indicate genes selected for ChIP assays. *F*, ChIP assays for H3K27me3 of the indicated genes in testis of tamoxifen-treated CTR mice of 6 weeks. ChIPs with IgGs served as negative controls. *Cdc6* gene was used as non-PcG target control gene. ChIP enrichments were calculated as a percentage of the total input signal ($n = 6$ animals per experimental group). *G*, comparison of the H3K27me3 ChIP data between CTR and iKO mice. H3K27me3 levels in the iKOs are represented as relative enrichment ($n = 6$ animals per experimental group). The data of the CTRs are expressed as a % of 1 CTR value. Data are represented as mean ± S.D. *, $p < 0.05$; **, $p < 0.01$; ***, $p < 0.001$.

expression or function. However, we noted that the CDK1/2 phosphorylation sites of EZH2 that control its chromatin targeting and degradation (Thr-345 and Thr-487) are not conserved in EZH1. Hence, the regulation of EZH1 and EZH2 by PP1:NIPP1 cannot be identical. At present, we cannot exclude either that the hampered dephosphorylation of other NIPP1 FHA ligands also contributes to the testis phenotype of the NIPP1 iKOs.

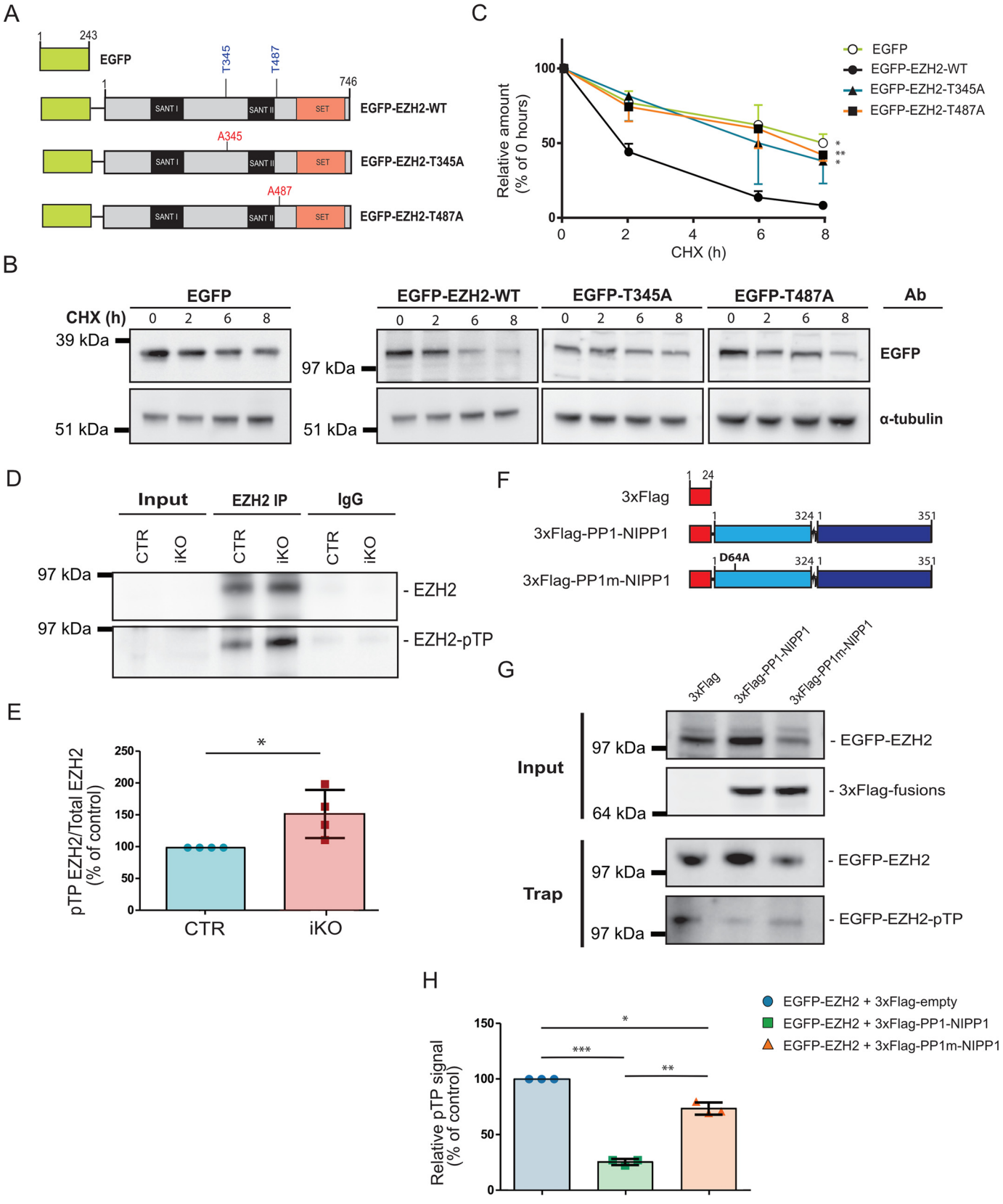

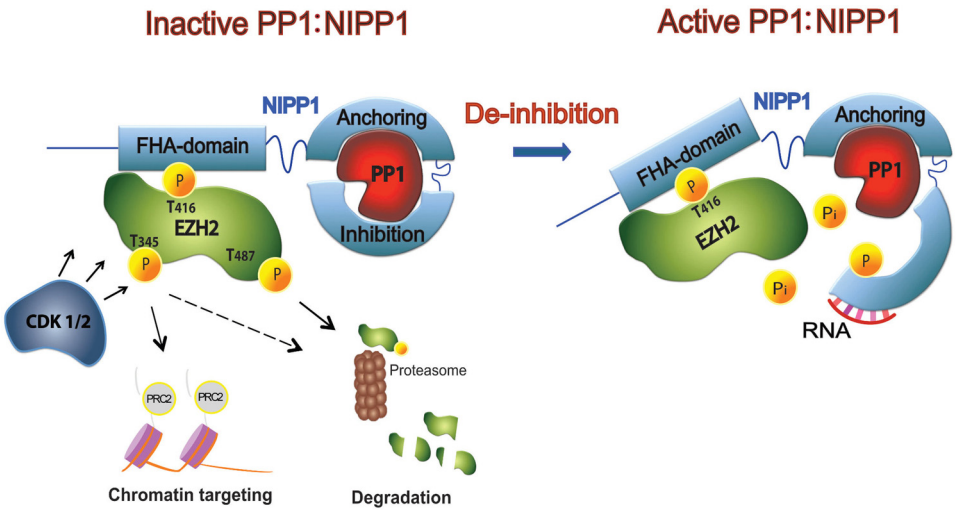

Figure 4. Model of the regulation of EZH2 by CDKs and PP1:NIPP1. CDKs phosphorylate EZH2 at Thr-345, Thr-416, and Thr-487. Thr-345 phosphorylation targets EZH2 to chromatin via noncoding RNAs, whereas Thr-487 (and prolonged Thr-345) phosphorylation results in the proteasomal degradation of EZH2. The phosphorylation of EZH2 at Thr-416 creates a docking site for the N-terminal FHA domain of NIPP1. EZH2-recruited NIPP1 prevents the immediate dephosphorylation of EZH2 by PRC2-associated PP1. However, the inhibition of PP1 by NIPP1 can be alleviated (de-inhibition) by the allosteric disruption of the interaction between PP1 and the C-terminal PP1-inhibitory domain of NIPP1, resulting in the dephosphorylation of EZH2. *In vitro*, such de-inhibition is seen after the binding of RNA to the C terminus of NIPP1 and after tyrosine phosphorylation of the C terminus. Note that, even when de-inhibited, NIPP1 remains tightly associated with PP1 via its PP1-anchoring domain.

In conclusion, we have identified EZH2 as an *in vivo* substrate of PP1:NIPP1. In the absence of NIPP1, a functional PP1:NIPP1 holoenzyme cannot be formed, resulting in the hyperphosphorylation and destabilization of EZH2.

Experimental procedures

Materials and methods

The following antibodies were used: Anti-NIPP1 (Sigma, HPA027452), anti-EZH2 (Cell Signaling Technology, 5246), anti-EZH2 (homemade) (12), anti-EZH2 (Cell Signaling Technology, 3147), anti-SUZ12 (Abcam, ab12073), anti-RBAP48 (GeneTex Inc., GTX0232), anti-TBP (Abcam, ab51841), anti–Pan-pTP (Cell Signaling Technology, 9391), anti-H3K27me3 (Upstate Biotechnology Inc., 07-449), anti-H3 (Santa Cruz Biotechnology, SC10809), anti-α-tubulin (Sigma-Aldrich, T6074), anti-EGFP (Santa Cruz Biotechnology, SC-8334), and anti-FLAG (Sigma-Aldrich, F7425).

Treatment of mice

NIPP1 (*Ppp1r8*) knockout mice were generated as described previously (27). All experimental protocols were approved by the KU Leuven Ethical Committee and were in accordance with the local Guide of Care of Experimental Animals. Both *Ubc-Cre-ERT2*$^{+/-}$;*Pppr8*$^{fl/+}$ control (CTR) and *Ubc-Cre-ERT2*$^{+/-}$;*Pppr8*$^{fl/-}$ inducible knockout (iKO) mice were treated postnatally (4-week-old mice) with 0.2 mg tamoxifen/g body weight (Sigma-Aldrich), as described previously, to induce the excision of the promoter region as well as exons 1 and 2 of the floxed *Ppp1r8* allele (27). Testes were harvested from anesthetized animals 2 weeks after tamoxifen treatment and either frozen in liquid nitrogen or fixed in Bouin's (Sigma-Aldrich) for a period of 6 h.

Immunohistochemistry

Fixed testes were embedded in paraffin and sectioned at a thickness of 6 μm. Testis sections were stained using the indicated antibodies and the TSA® Fluorescein System (Perkin-Elmer). Immunofluorescence images were acquired with a Leica TCS SPE laser scanning confocal microscope.

Cell culture

C18-4 spermatogonial cells were cultured in high-glucose Dulbecco's modified Eagle's medium/F12, supplemented with 10% fetal bovine serum, 100 units/ml penicillin, and 100 μg/ml streptomycin. Transfections were performed using Lipofectamine 2000 (Invitrogen) or jetPRIME kit (Polyplus). Cycloheximide (Sigma-Aldrich) was used at a concentration of 50 μg/ml for the indicated times and nocodazole (Sigma-Aldrich) at a concentration of 0.3 μg/ml for 16 h.

Figure 3. NIPP1 controls the dephosphorylation and stability of EZH2. *A*, schematic representation of EGFP and the indicated EGFP-tagged EZH2 variants. *B*, nonsynchronized C18-4 cells were transfected with EGFP or the indicated EGFP-tagged EZH2 variants and treated with cycloheximide (*CHX*) (50 μg/ml) for the indicated time points. The fate of EGFP and the EGFP fusions was determined by immunoblotting with an anti-EGFP antibody. Representative example of the turnover of EGFP and EGFP-EZH2 fusions in the presence of cycloheximide. α-Tubulin was used as a loading control. *Ab*, antibody used. *C*, quantification of *panel B* represented as mean ± S.D. ($n = 3$ independent experiments). *, $p < 0.05$; **, $p < 0.01$. *D*, EZH2 was immunoprecipitated (*IP*) from testis extracts of tamoxifen-treated mice of 6 weeks. The IP loading was corrected for equal amounts of immunoprecipitated EZH2 in the CTR and iKO conditions. IgGs were used as negative control. The blots were stained for total EZH2 and TP-dipeptide phosphorylated EZH2 (pTP). *E*, quantification of relative amounts of phosphorylated EZH2, as shown in *panel D* ($n = 4$ animals per experimental group). *, $p < 0.05$. *F*, scheme of FLAG and FLAG-tagged PP1-NIPP1 and PP1m-NIPP1 fusions. *G*, EGFP-EZH2 and either FLAG, FLAG-PP1-NIPP1, or FLAG-PP1m-NIPP1 were transiently expressed in the C18-4 spermatogonial cells for 48 h. The cells were arrested in prometaphase by a treatment with nocodazole for 16 h. Cell lysates were analyzed for the presence of EGFP-EZH2 and FLAG-PP1-NIPP1 or FLAG-PP1m-NIPP1. EGFP-traps were immunoblotted for EGFP-EZH2 and phosphorylated EZH2 (pTP). *, $p < 0.05$. *H*, quantification of the relative amounts of phosphorylated EZH2 as shown in *panel G* ($n = 3$ independent experiments). *, $p < 0.05$; **, $p < 0.01$, **, $p < 0.001$.

Plasmids

Plasmids encoding EGFP-tagged mouse WT EZH2, EZH2-T345A and EZH2-T487A, and FLAG-tagged WT PP1-NIPP1 fusion and its hypoactive mutant (PP1m-NIPP1) have been described (12, 22, 38).

Biochemical procedures

Testes were homogenized using a Dounce homogenizer (Sigma-Aldrich) and incubated for 20 min at 4 °C in lysis buffer containing modified RIPA buffer (50 mM Tris-HCl at pH 7.4, 1% Triton X-100, 0.2% sodium deoxycholate, 0.2% SDS, 1 mM EDTA, and 0.3 M NaCl). Lysate supernatant was used for immunoblotting or immunoprecipitation. To examine the interaction between NIPP1 and EZH2, testis nuclear extracts were prepared as described by Prieto *et al.* (41). All lysis buffers were supplemented with 20 mM NaF, 5 μM leupeptin, 0.5 mM phenylmethanesulfonyl fluoride, 0.5 mM benzamidine, and 1 mM orthovanadate. For immunoprecipitation assays in testis extracts, the supernatant was precleared with 30 μl of protein A Sepharose beads (1:1 suspension in TBS) for 1 h at 4 °C. After centrifugation (30 s at 425 × *g*) the supernatant was incubated overnight at 4 °C with antibodies against EZH2 or anti-mouse IgG for control (Dako). Subsequently, 30 μl of protein A Sepharose (1:1 suspension in TBS) was added for 1 h at 4 °C. After centrifugation for 30 s at 425 × *g*, the pellet was washed five times with Tris-buffered saline (TBS), supplemented with 0.1% Triton X-100, and 0.25% Nonidet P-40, and subjected to SDS-PAGE.

C18-4 cells were harvested and lysed for 30 min at 4 °C in lysis buffer containing 50 mM Tris-HCl at pH 7.4, 0.3 M NaCl, 0.5% Triton X-100, 20 mM NaF, 5 μM leupeptin, 0.5 mM phenylmethanesulfonyl fluoride, 0.5 mM benzamidine, and 1 mM orthovanadate. After centrifugation (10 min at 1800 × *g*), the supernatant was used for immunoblotting or EGFP-trapping (39). Immunoblotting (10% SDS-PAGE) was performed with the indicated antibodies. Immunoblots were visualized using ECL reagent (PerkinElmer) in an ImageQuant LAS4000 imaging system (GE Healthcare) and were quantified using ImageQuant TL software (GE Healthcare).

Chromatin immunoprecipitation

ChIP assays were performed according to the protocol of Upstate, as described (20). Briefly, 100 mg of testis homogenate was cross-linked with 1% paraformaldehyde and the pellet was resuspended in SDS lysis buffer (50 mM Tris/HCl at pH 8.0, 1% SDS, 10 mM EDTA), supplemented with 20 mM NaF, 5 μM leupeptin, 0.5 mM phenylmethanesulfonyl fluoride, 0.5 mM benzamidine, and 1 mM orthovanadate. The pellet was sonicated with 30 s on/30 s off cycles for 35 min. 500 μg of sheared chromatin (A_{260}) was precleared with protein A Sepharose and blocked with 1 mg/ml BSA, 1 mg/ml salmon sperm DNA, and 1% Triton X-100. 150 μg of precleared chromatin was incubated with anti-H3K27me3 antibody or with polyclonal rabbit anti-mouse Igs (IgG). The histone/DNA complex was eluted with elution buffer (0.1 M $NaHCO_3$ at pH 8.0, 1% SDS) and after reversing the cross-links, the DNA was purified using the GenElute™ PCR Clean-Up Kit (Sigma-Aldrich).

The immunoprecipitated DNA was quantified by real-time qPCR. Gene-specific primers for ChIP–quantitative real-time PCR analysis are listed (Fig. S1). Selection of the likely PcG target genes was performed by a comparative analysis of the top list (Log_2 (FC) $> \pm 0.58$; false discovery rate < 0.05) genes derived from RNA-Seq data and a list composed of PcG target genes that were described previously (5, 32–34).

Statistics

Statistically significant differences between the experimental and control groups were analyzed with the GraphPad Prism software using two-way unpaired (Fig. 1, *B–F*; Fig. 2, *C* and *G*; Fig. 3*E*) or paired (Fig. 3, *C* and *H*) Student's *t* test. The heat map shown in Fig. 2*E* was constructed based on a Spearman's correlation between the samples using the normalized FPKM values as expression values. The heat map shows the unsupervised clustering of the genes and the samples. The z-score was used to normalize the values per gene and for the color gradient.

Author contributions—M. Ferreira and M. B. conceptualization; M. Ferreira and I. V. resources; M. Ferreira and A. V. E. data curation; M. Ferreira software; M. Ferreira formal analysis; M. Ferreira validation; M. Ferreira investigation; M. Ferreira and A. V. E. visualization; M. Ferreira, A. V. E., and M. B. methodology; M. Ferreira and M. B. writing-original draft; M. Ferreira, A. V. E., and M. B. writing-review and editing; M. Fardilha and M. B. funding acquisition; M. Fardilha and M. B. project administration; A. V. E. and M. B. supervision.

Acknowledgments—We thank Prof. Dr. Marie-Claude Hofmann for kindly providing the C18-4 cell line. We thank Maud De Meyer, Annemie Hoogmartens, and Fabienne Withof for technical assistance. We acknowledge Prof. M. Baes (KU Leuven, Belgium) for the donation of UBC-Cre-ERT2 mice. Library preparation, RNA-Seq, and statistical analysis was performed at the VIB Nucleomics Core.

References

1. Sasaki, H., and Matsui, Y. (2008) Epigenetic events in mammalian germ-cell development: Reprogramming and beyond. *Nat. Rev. Genet.* **9,** 129–140 CrossRef Medline
2. Kubo, N., Toh, H., Shirane, K., Shirakawa, T., Kobayashi, H., Sato, T., Sone, H., Sato, Y., Tomizawa, S., Tsurusaki, Y., Shibata, H., Saitsu, H., Suzuki, Y., Matsumoto, N., Suyama, M., Kono, T., Ohbo, K., and Sasaki, H. (2015) DNA methylation and gene expression dynamics during spermatogonial stem cell differentiation in the early postnatal mouse testis. *BMC Genomics* **16,** 624 CrossRef Medline
3. Ly, L., Chan, D., and Trasler, J. M. (2015) Developmental windows of susceptibility for epigenetic inheritance through the male germline. *Semin. Cell Dev. Biol.* **43,** 96–105 CrossRef Medline
4. Komai, Y., Tanaka, T., Tokuyama, Y., Yanai, H., Ohe, S., Omachi, T., Atsumi, N., Yoshida, N., Kumano, K., Hisha, H., Matsuda, T., and Ueno, H. (2014) Bmi1 expression in long-term germ stem cells. *Sci. Rep.* **4,** 6175 CrossRef Medline
5. Mu, W., Starmer, J., Fedoriw, A. M., Yee, D., and Magnuson, T. (2014) Repression of the soma-specific transcriptome by polycomb-repressive complex 2 promotes male germ cell development. *Genes Dev.* **28,** 2056–2069 CrossRef Medline
6. Mu, W., Starmer, J., Shibata, Y., Yee, D., and Magnuson, T. (2017) EZH1 in germ cells safeguards the function of PRC2 during spermatogenesis. *Dev. Biol.* **424,** 198–207 CrossRef Medline
7. Sparmann, A., and van Lohuizen, M. (2006) Polycomb silencers control cell fate, development and cancer. *Nat. Rev. Cancer* **6,** 846–856 CrossRef Medline
8. Aranda, S., Mas, G., and Di Croce, L. (2015) Regulation of gene transcription by Polycomb proteins. *Sci. Adv.* **1,** e1500737 CrossRef Medline

9. Comet, I., and Helin, K. (2014) Revolution in the Polycomb hierarchy. *Nat. Struct. Mol. Biol.* **21,** 573–575 CrossRef Medline
10. Chen, S., Bohrer, L. R., Rai, A. N., Pan, Y., Gan, L., Zhou, X., Bagchi, A., Simon, J. A., and Huang, H. (2010) Cyclin-dependent kinases regulate epigenetic gene silencing through phosphorylation of EZH2. *Nat. Cell Biol.* **12,** 1108–1114 CrossRef Medline
11. Kaneko, S., Li, G., Son, J., Xu, C. F., Margueron, R., Neubert, T. A., and Reinberg, D. (2010) Phosphorylation of the PRC2 component Ezh2 is cell cycle-regulated and up-regulates its binding to ncRNA. *Genes Dev.* **24,** 2615–2620 CrossRef Medline
12. Minnebo, N., Görnemann, J., O'Connell, N., Van Dessel, N., Derua, R., Vermunt, M. W., Page, R., Beullens, M., Peti, W., Van Eynde, A., and Bollen, M. (2013) NIPP1 maintains EZH2 phosphorylation and promoter occupancy at proliferation-related target genes. *Nucleic Acids Res.* **41,** 842–854 CrossRef Medline
13. Yang, C. C., LaBaff, A., Wei, Y., Nie, L., Xia, W., Huo, L., Yamaguchi, H., Hsu, Y. H., Hsu, J. L., Liu, D., Lang, J., Du, Y., Lien, H. C., Li, L. Y., Deng, R., Chan, L. C., Yao, J., Kleer, C. G., Hortobagyi, G. N. H. M. (2015) Phosphorylation of EZH2 at T416 by CDK2 contributes to the malignancy of triple negative breast cancers. *Am. J. Transl. Res.* **7,** 1009–1020 Medline
14. Wu, S. C., and Zhang, Y. (2011) Cyclin-dependent kinase 1 (CDK1)-mediated phosphorylation of enhancer of zeste 2 (Ezh2) regulates its stability. *J. Biol. Chem.* **286,** 28511–28519 CrossRef Medline
15. Wei, Y., Chen, Y.-H., Li, L.-Y., Lang, J., Yeh, S.-P., Shi, B., Yang, C.-C., Yang, J.-Y., Lin, C.-Y., Lai, C.-C., and Hung, M.-C. (2011) CDK1-dependent phosphorylation of EZH2 suppresses methylation of H3K27 and promotes osteogenic differentiation of human mesenchymal stem cells. *Nat. Cell Biol.* **13,** 87–94 CrossRef Medline
16. Sahasrabuddhe, A. A., Chen, X., Chung, F., Velusamy, T., Lim, M. S., and Elenitoba-Johnson, K. S. J. (2015) Oncogenic Y641 mutations in EZH2 prevent Jak2/β-TrCP-mediated degradation. *Oncogene* **34,** 445–454 CrossRef Medline
17. Jin, Q., Van Eynde, A., Beullens, M., Roy, N., Thiel, G., Stalmans, W., and Bollen, M. (2003) The protein phosphatase-1 (PP1) regulator, nuclear inhibitor of PP1 (NIPP1), interacts with the polycomb group protein, embryonic ectoderm development (EED), and functions as a transcriptional repressor. *J. Biol. Chem.* **278,** 30677–30685 CrossRef Medline
18. Roy, N., Van Eynde, A., Beke, L., Nuytten, M., and Bollen, M. (2007) The transcriptional repression by NIPP1 is mediated by Polycomb group proteins. *Biochim. Biophys. Acta* **1769,** 541–545 CrossRef Medline
19. Nuytten, M., Beke, L., Van Eynde, A., Ceulemans, H., Beullens, M., Van Hummelen, P., Fuks, F., and Bollen, M. (2008) The transcriptional repressor NIPP1 is an essential player in EZH2-mediated gene silencing. *Oncogene* **27,** 1449–1460 CrossRef Medline
20. Van Dessel, N., Beke, L., Görnemann, J., Minnebo, N., Beullens, M., Tanuma, N., Shima, H., Van Eynde, A., and Bollen, M. (2010) The phosphatase interactor NIPP1 regulates the occupancy of the histone methyltransferase EZH2 at Polycomb targets. *Nucleic Acids Res.* **38,** 7500–7512 CrossRef Medline
21. Nishioka, K., Miyazaki, H., and Soejima, H. (2018) Unbiased shRNA screening, using a combination of FACS and high-throughput sequencing, enables identification of novel modifiers of Polycomb silencing. *Sci. Rep.* **8,** 12128 CrossRef Medline
22. Winkler, C., Rouget, R., Wu, D., Beullens, M., Van Eynde, A., and Bollen, M. (2018) Overexpression of PP1–NIPP1 limits the capacity of cells to repair DNA double-strand breaks. *J. Cell Sci.* **131,** jcs214932 CrossRef Medline
23. Heroes, E., Lesage, B., Görnemann, J., Beullens, M., Van Meervelt, L., and Bollen, M. (2013) The PP1 binding code: A molecular-lego strategy that governs specificity. *FEBS J.* **280,** 584–595 CrossRef Medline
24. Beullens, M., Vulsteke, V., Van Eynde, A., Jagiello, I., Stalmans, W., and Bollen, M. (2000) The C-terminus of NIPP1 (nuclear inhibitor of protein phosphatase-1) contains a novel binding site for protein phosphatase-1 that is controlled by tyrosine phosphorylation and RNA binding. *Biochem. J.* **352,** 651–658 Medline
25. Tanuma, N., Kim, S. E., Beullens, M., Tsubaki, Y., Mitsuhashi, S., Nomura, M., Kawamura, T., Isono, K., Koseki, H., Sato, M., Bollen, M., Kikuchi, K., and Shima, H. (2008) Nuclear inhibitor of protein phosphatase-1 (NIPP1) directs protein phosphatase-1 (PP1) to dephosphorylate the U2 small nuclear ribonucleoprotein particle (snRNP) component, spliceosome-associated protein 155 (Sap155). *J. Biol. Chem.* **283,** 35805–35814 CrossRef Medline
26. Van Dessel, N., Boens, S., Lesage, B., Winkler, C., Görnemann, J., Van Eynde, A., and Bollen, M. (2015) Protein phosphatase PP1-NIPP1 activates mesenchymal genes in HeLa cells. *FEBS Lett.* **589**, 1314–1321 CrossRef Medline
27. Ferreira, M., Boens, S., Winkler, C., Szekér, K., Verbinnen, I., Van Eynde, A., Fardilha, M., and Bollen, M. (2017) The protein phosphatase 1 regulator NIPP1 is essential for mammalian spermatogenesis. *Sci. Rep.* **7,** 13364 CrossRef Medline
28. Cao, R., and Zhang, Y. (2004) SUZ12 is required for both the histone methyltransferase activity and the silencing function of the EED-EZH2 complex. *Mol. Cell* **15,** 57–67 CrossRef Medline
29. Cao, R., and Zhang, Y. (2004) The functions of E(Z)/EZH2-mediated methylation of lysine 27 in histone H3. *Curr. Opin. Genet. Dev.* **14,** 155–164 CrossRef Medline
30. Pasini, D., Bracken, A. P., Jensen, M. R., Lazzerini Denchi, E., and Helin, K. (2004) Suz12 is essential for mouse development and for EZH2 histone methyltransferase activity. *EMBO J.* **23,** 4061–4071 CrossRef Medline
31. Montgomery, N. D., Yee, D., Chen, A., Kalantry, S., Chamberlain, S. J., Otte, A. P., and Magnuson, T. (2005) The murine polycomb group protein Eed is required for global histone H3 lysine-27 methylation. *Curr. Biol.* **15,** 942–947 CrossRef Medline
32. Bracken, A. P., Dietrich, N., Pasini, D., Hansen, K. H., and Helin, K. (2006) Genome-wide mapping of polycomb target genes unravels their roles in cell fate transitions. *Genes Dev.* **20,** 1123–1136 CrossRef Medline
33. Lee, T. I., Jenner, R. G., Boyer, L. A., Guenther, M. G., Levine, S. S., Kumar, R. M., Chevalier, B., Johnstone, S. E., Cole, M. F., Isono, K.-I., Koseki, H., Fuchikami, T., Abe, K., Murray, H. L., Zucker, J. P., *et al.* (2006) Control of developmental regulators by Polycomb in human embryonic stem cells. *Cell* **125,** 301–313 CrossRef Medline
34. Squazzo, S. L., O'Geen, H., Komashko, V. M., Krig, S. R., Jin, V. X., Jang, S. W., Margueron, R., Reinberg, D., Green, R., and Farnham, P. J. (2006) Suz12 binds to silenced regions of the genome in a cell-type-specific manner. *Genome Res.* **16,** 890–900 CrossRef Medline
35. Xu, K., Wu, Z. J., Groner, A. C., He, H. H., Cai, C., Lis, R. T., Wu, X., Stack, E. C., Loda, M., Liu, T., Xu, H., Cato, L., Thornton, J. E., Gregory, R. I., Morrissey, C., *et al.* (2012) EZH2 oncogenic activity in castration-resistant prostate cancer cells is polycomb-independent. *Science* **338,** 1465–1469 CrossRef Medline
36. Vasanthakumar, A., Xu, D., Lun, A. T., Kueh, A. J., van Gisbergen, K. P., Iannarella, N., Li, X., Yu, L., Wang, D., Williams, B. R., Lee, S. C., Majewski, I. J., Godfrey, D. I., Smyth, G. K., Alexander, W. S., Herold, M. J., Kallies, A., Nutt, S. L., and Allan, R. S. (2017) A non-canonical function of Ezh2 preserves immune homeostasis. *EMBO Rep.* **18,** 619–631 CrossRef Medline
37. Ardehali, M. B., Anselmo, A., Cochrane, J. C., Kundu, S., Sadreyev, R. I., and Kingston, R. E. (2017) Polycomb repressive complex 2 methylates Elongin A to regulate transcription. *Mol. Cell* **68,** 872–884.e6 CrossRef Medline
38. Wu, D., De Wever, V., Derua, R., Winkler, C., Beullens, M., Van Eynde, A., and Bollen, M. (2018) A substrate-trapping strategy for protein phosphatase PP1 holoenzymes using hypoactive subunit fusions. *J. Biol. Chem.* **293,** 15152–15162 CrossRef Medline
39. Winkler, C., De Munter, S., Van Dessel, N., Lesage, B., Heroes, E., Boens, S., Beullens, M., Van Eynde, A., and Bollen M (2015) The selective inhibition of protein phosphatase-1 results in mitotic catastrophe and impaired tumor growth. *J. Cell Sci.* **128,** 4526–4537 CrossRef Medline
40. Ferreira, M., Beullens, M., Bollen, M., and Van Eynde, A. (2018) Functions and therapeutic potential of protein phosphatase 1: Insights from mouse genetics. *Biochim. Biophys. Acta Mol. Cell Res.* 10.1016/j.bbamcr.2018.07.019 CrossRef Medline
41. Prieto, I., Suja, J. A., Pezzi, N., Kremer, L., Martínez-A., C., Rufas, J. S., and Barbero, J. L. (2001) Mammalian STAG3 is a cohesin specific to sister chromatid arms in meiosis I. *Nat. Cell Biol.* **3,** 761–766 CrossRef Medline